Journal of Alloys and Compounds 526 (2012) 145–150

Contents lists available at SciVerse ScienceDirect

Journal of Alloys and Compounds

journal homepage: www.elsevier.com/locate/jallcom

An amperometric NO_2 sensor based on nano-structured $La_{0.75}Sr_{0.25}Cr_{0.5}Mn_{0.5}O_{3-\delta}$ prepared by impregnating method

L. Dai [a,b], L. Wang [b,*], G.J. Shao [a], Y.H. Li [b], Z.C. Hao [b]

[a] College of Environmental and Chemical Engineering, Yanshan University, Qinhuangdao 066004, PR China
[b] College of Chemical Engineering, Hebei United University, Tangshan 063009, PR China

ARTICLE INFO

Article history:
Received 3 January 2012
Received in revised form 31 January 2012
Accepted 3 February 2012
Available online xxx

Keywords:
NO_2 sensor
Amperometric
Impregnating method
Nano-structure
$La_{0.75}Sr_{0.25}Cr_{0.5}Mn_{0.5}O_{3-\delta}$

ABSTRACT

An amperometric NO_2 sensor using nano-structured perovskite-type oxide $La_{0.75}Sr_{0.25}Cr_{0.5}Mn_{0.5}O_{3-\delta}$ (LSCM) as sensing electrode with $Ce_{0.9}Gd_{0.1}O_{1.95}$ (CGO)electrolyte was fabricated. The LSCM particles were prepared in the porous CGO layer by impregnating method. The composition and microstructure of the sample were characterized by XRD and SEM, respectively. The properties of the sensor for monitoring NO_2 were studied. The results showed that the LSCM particles in the range of 50–150 nm were homogeneously dispersed in the porous CGO layer. The response current was almost linear to NO_2 concentration in the range between 20 and 300 ppm. With the temperatures increasing, the sensitivity increased and reached 111.36 nA ppm^{-1} at 500 °C. The sensor showed good response, recovery, reproducibility and stability. Although the response current was slightly affected by changing O_2 concentrations in the range of 0–10 vol%, the influence was negligibly small.

1. Introduction

Nitrogen dioxide (NO_2), which is emitted from the exhaust gas of automotive engines, boilers, and any other combustion facilities into the atmosphere, is one of the main causes of air pollution and highly harmful for human beings [1,2]. Therefore, it is necessary to develop high performance NO_2 sensors for monitoring the exhaust gas from automobiles and factories. For this purpose, a special attention has been paid to the solid electrolyte type NO_2 sensors which are available on detection of NO_2 using either the potentiometric [3–8], the impedancemetric [9–14] or the amperometric mode [15–20] with fast response, high sensibility and good stability.

In order to improve the properties of the NO_2 sensors further, nano-structured sensing electrodes have attracted many interests of researchers [21–24]. It has been proposed that the utilization of nano-structured sensing electrodes means the increasing length of the triple phase boundary (gas/sensing electrode/electrolyte) and high catalytic activities to NO_2, which leads to improve the sensitivity, stability and anti-interference. Plashnitsa et al. [21,22] reported the novel mixed-potential-type planar sensors using nano-structured NiO-Ses, which obtain a large enhancement in both sensitivity and selectivity to NO_2. Xiong and Kale [23] used nano-structured $CuO + CuCr_2O_4$ mixed-oxides as sensing electrode. The EMF (electromotive force) response of the sensor was highly reproducible to change in concentration of NO_2 and the sensor also showed negligible cross-sensitivity to O_2, CO and CH_4. Martin et al. [24] investigated an impedancemetric method for NO_2 sensing using nano-sized YSZ (yttria-stabilized zirconia)/Cr_2O_3 composite electrodes and found that the sensing performance of the sensor was affected by the surface topography of sensing electrodes. In the meanwhile, the triple phase boundary also can be increased by designing and controlling the surface roughness of the electrolyte. Liang et al. [25] fabricated a mixed-potential-type NO_2 sensor using YSZ plate corroded by hydrofluoric acid as electrolyte to increase the triple phase boundary and the selectivity and rapid response–recovery characteristics of the NO_2 sensor were improved.

As mentioned above, the nano-structured sensing electrodes can improve performance of potentiometric and impedancemetric sensors. It is reasonable that the nano-structured sensing electrodes should also be used to enhance characteristics of the amperometric NO_2 sensor. In this paper, an amperometric NO_2 sensor based on measuring currents upon application of a cathodic potential to nano-structured LSCM sensing electrode and Pt counter electrode on a CGO electrolyte for detecting NO_2 was proposed. The nano-structured LSCM particles were prepared in the porous CGO layer by impregnating method which is a well-known method in the development of heterogeneous catalysts for solid oxide fuel cells [26–29]. The detailed sensing characteristics of the sensor are reported and discussed here.

* Corresponding author. Tel.: +86 315 2592170; fax: +86 315 2592170.
E-mail address: tswling@126.com (L. Wang).

0925-8388/$ – see front matter © 2012 Elsevier B.V. All rights reserved.
doi:10.1016/j.jallcom.2012.02.101

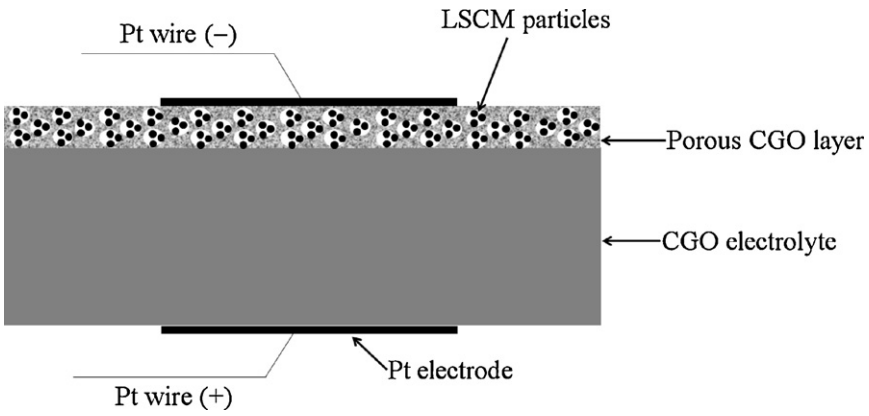

Fig. 1. Schematic view of the sensor.

2. Experimental

2.1. Preparation of CGO electrolyte and its porous CGO layer

Analytically pure CeO_2 and Gd_2O_3 were mixed with ethanol and ball-milled for 24 h and then calcined at 950 °C for 5 h in air. The milling-calcining cycle was repeated for three times. The calcined powders were pressed into pellets (about 10 mm in diameter, 2 mm thickness) and then sintered at 1600 °C for 5 h to form dense CGO electrolyte.

The porous CGO layer on the surface of above-mentioned dense CGO pellets was prepared by screen printing technique and then sintered at 1450 °C for 5 h. The ink used in screen-printing was prepared by dispersing CGO powder with 30 wt.% pore-forming agent (graphite powder) into an organic vehicle (terpineol, 94 wt.% and ethylcellulose, 6 wt.%).

2.2. Sensor fabrication and characterization

The LSCM nanoparticles used as sensing materials were introduced into the Porous CGO layer by impregnating technique. Firstly, 1 mol L^{-1} LSCM precursor solution for impregnation was prepared by adding $La(NO_3)_3{\cdot}6H_2O$, $Sr(NO_3)_2$, $Cr(NO_3)_3{\cdot}9H_2O$ and $Mn(NO_3)_2{\cdot}4H_2O$ to deionized water according to molar ratio 0.75:0.25:0.5:0.5. Secondly, the LSCM precursor solution was pipetted into porous layer of the samples with 4 μL of solution at a time, followed by drying in an oven at 100 °C. The impregnating-drying cycle was repeated for five times. After impregnation, the sample was calcined at 800 °C for 3 h in air to decompose nitrate salts and produce the perovskite LSCM phase. The LSCM loading was about 4.6 mg. Pt paste was painted on the two sides of sample. Pt wires were used to make contact with the sensor, as shown in Fig. 1. The composition and microstructure of the sample were characterized by X-ray diffraction with Cu-Kα radiation (XRD, D/MAX2500PC) and field emission scanning electron microscopy (SEM, S-4800), respectively.

2.3. Evaluation of sensing properties

NO_2 sensing properties were tested in a gas flow apparatus with heating tube furnace in the temperature range 400–550 °C. The gas environment consisted of a changing concentration of NO_2 (0–300 ppm) with base gases ($O_2 + N_2$ balance) at a total flow rate of 100 cm^3/min. The current–potential characteristics of sensors were measured by potentiodynamic method at a constant scan-rate of 1 mV/s in the potential rang from 0 to −300 mV by using a two-electrode configuration. The amperometric responses of the sensor were measured by potentiostatic method at −300 mV. The complex-impedance measurements of the sensor were performed in the frequency range of 0.1–1 MHz with a 50 mV amplitude ac signal. The fore-mentioned all electrochemical measurements were performed by the electrochemical work station (Zahner IM6e).

3. Results and discussion

3.1. Characterization of the sensor materials

Fig. 2 shows the XRD patterns of the porous layer without and with LSCM-impregnation. The porous framework displayed a single CGO phase before LSCM-impregnation (Fig. 2A). There was no peak of carbon as pore-former in XRD pattern, which manifested that carbon had been removed during sintering process. After impregnation and fired at 800 °C for 3 h, perovskite LSCM phase can form and no other phase appears (Fig. 2B).

SEM micrographs of surfaces and fractured cross-sections of the sensor without and with LSCM-impregnation are shown in Fig. 3. The original CGO porous layer showed a uniform, porous and three-dimensional network structure with sub-micron pores (Fig. 3A), which was a result due to the oxidation of pore-forming agent (graphite powder). As seen in Fig. 3B, the porous layer was combined with dense CGO solid electrolyte substrate tightly after sintering. The thickness of porous layer after 3 times printing was about 25–30 μm. After LSCM impregnation, the representative SEM images of surface and cross-section of the sensing electrode are shown in Fig. 3C and D. It was seen that the LSCM particles were uniformly dispersed in the CGO backbone and deposited not only on the surface of the porous layer but also throughout the CGO backbone. Very fine LSCM particles were formed around CGO backbone and their size was in the range of 50–150 nm (Fig. 3E). Because sensing material LSCM made contact with CGO electrolyte in three-dimensional structure, the triple phase boundary length (the NO_2 gas/LSCM electrode/CGO electrolyte) was greatly enhanced, which means increasing number of gas reaction sites and brings about the improvement of the response for the sensor. It is speculated that the sample gas can diffuse easily into the SE layer due to its high porosity and NO_2 gas can be easily reduced because of the presence of monodispersed nanocrystalline LSCM particles.

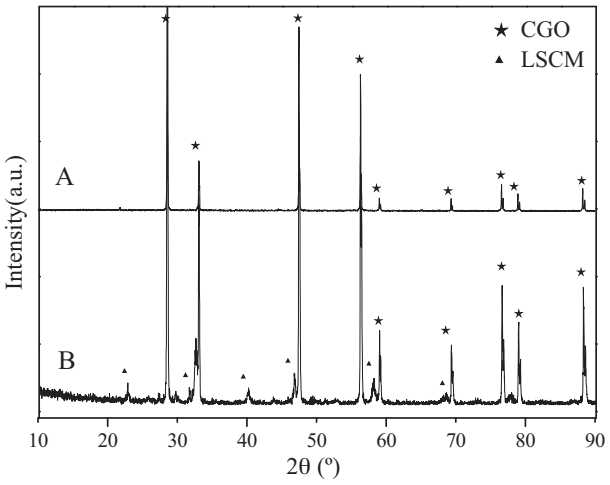

Fig. 2. XRD patterns of the porous layer without (A) and with (B) LSCM-impregnation.

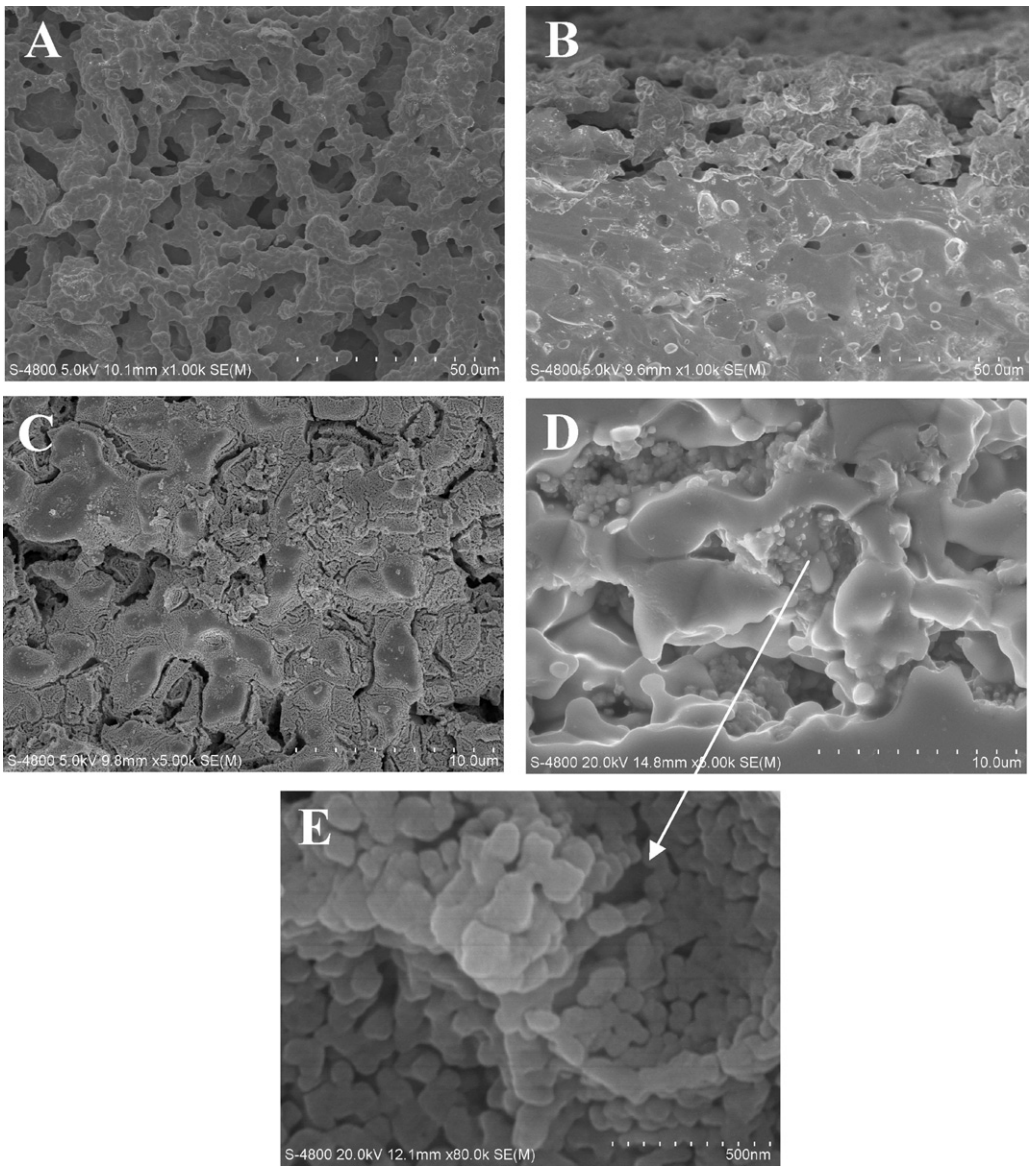

Fig. 3. SEM images of the samples: (A) the surface without LSCM-impregnation, (B) cross-section without LSCM-impregnation, (C) the surface with LSCM-impregnation, (D) cross-section with LSCM-impregnation, (E) LSCM particles.

3.2. Sensing performances of the sensor

This sensor can be described by the following electrochemical cells in sample gas: (−) $O_2 + NO_2$, LSCM/CGO/Pt, $NO_2 + O_2$ (+). When the potential moves negatively from the open potential, the following electrochemical reactions will occur:

$$\text{Cathode}: \quad NO_2 + 2e^- \rightarrow NO + O^{2-} \tag{1}$$

$$\text{Anode}: \quad 2O^{2-} \rightarrow O_2 + 4e^- \tag{2}$$

Fig. 4 shows the current–voltage (I–V) characteristics of the sensor. Potential scans from 0 to −300 mV were acquired for the sensor with a scan rate of 1 mV/s under various NO_2 concentrations and different operating temperatures. We can see from I–V curves that the response current value increased with the negatively moving of applied potential when temperature was fixed. Moreover, with the operating temperature increasing, the response current became larger at given NO_2 concentration. For example, the response currents to 300 ppm NO_2 reached about 7 μA and 120 μA at 400 and 550 °C, respectively. The current for the sensor was larger than that of the sensor using conventional sensing electrode [15,18]. At a fixed NO_2 concentration, the response current depends on catalytic activities of sensing material to reaction (1) and the length of the triple phase boundary where reaction (1) takes place. In present sensor, because of nano-sized LSCM particles dispersed in porous CGO backbone as sensing material, LSCM catalytic activity is not only enhanced, but also the length of the triple phase boundary is increased due to three-dimensional contact between CGO and LSCM.

In optimizing the sensor response, choices needed to be made involving the magnitude of polarization. The polarization promotes reaction (1), but the electrode degradation can arise from coarsening of electrode microstructure at large polarization [30]. In the meanwhile, polarization can also create morphological change of the sensing electrode [31]. So, choice of −300 mV for the cathodic polarization should minimize the electrode degradation and lead to a maximum current value in the polarization range.

The relationships between the response current and NO_2 concentrations at the bias potential of −300 mV are also shown in insets of Fig. 4. The response current was nearly linear change with NO_2

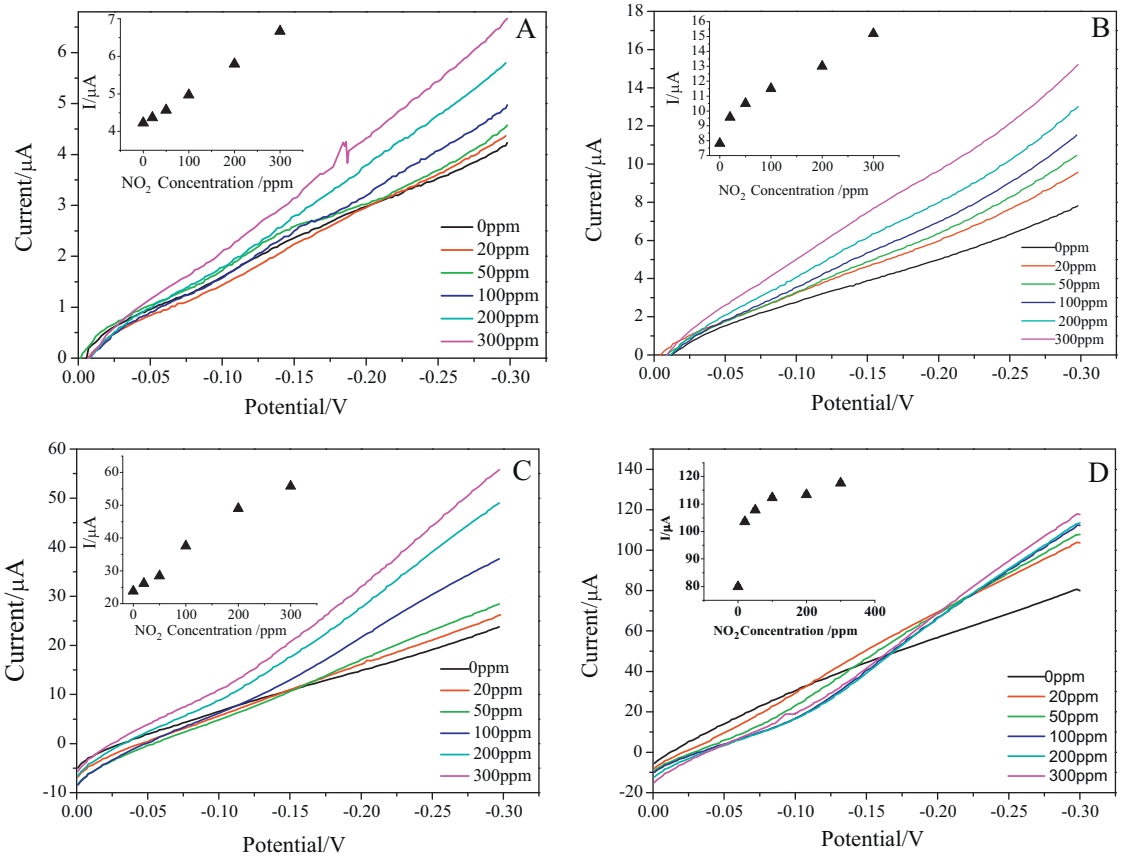

Fig. 4. *I–V* characteristics of the sensor with various NO_2 concentrations at 400 °C (A), 450 °C (B), 500 °C (C) and 550 °C (D).

concentration in the range between 20 and 300 ppm at 400–500 °C. With the operating temperature increasing, the sensitivity of the sensor increase and was evaluated to be 111.36 nA ppm^{-1} at 500 °C. However, at the operating temperature of 550 °C, there was not a linear relationship between the response current and NO_2 concentration. The sensitivity became lower than the one at 500 °C. The response current of the sensor stems from the electrochemical catalytic reduction of NO_2 at the triple phase boundary. With the temperature elevating, the chemical catalytic decomposition of NO_2 is increased, which results in the ratio of NO_2 by electrochemical catalytic reduction decreasing. Therefore, the sensitivity becomes lower.

Fig. 5 shows transient response curves of the sensor in NO_2 concentration from 20 to 300 ppm at 450 °C (Fig. 5A) and 500 °C (Fig. 5B), when the bias potential of −300 mV was applied. It was seen that the current values sharply increased from the base line upon switching from the base gas to the sample gas and the relatively steady current was finally attained. When the concentration of NO_2 was decreased to 0 ppm, the response current was reversibly returned to base line value. The sensor responded and recovered quickly as the NO_2 concentration was changed in every step and the base line keeps stable. The results shown in Fig. 5 were found to be highly reproducible when the concentration of NO_2 was switched between 0 and 300 ppm. The response time defined as time for reaching the 90% steady current is 220 s and the recovery time defined as time attaining within 10% of the initial current value is 360 s for 300 ppm NO_2 at 500 °C.

In addition, the response/recovery times are also influenced by the gas delivery system. Because of dead volume, it takes some time for the NO_2 concentrations in gas mixtures to reach a steady state in test chamber when NO_2 concentrations change step by step. In support of this argument, the response current varying with time for 200 ppm NO_2 at two different total gas flow rates (100 and 300 cm^3/min) at 500 °C was recorded and shown in Fig. 6. It can be seen that the response time was 350 s at a flow rate of 100 cm^3/min. When the total flow rate was increased to 300 cm^3/min, a 120 s response time was obtained. In fact, the real response/recovery time can be faster if the parameters of sensor fabrication, such as the thickness of the porous CGO layer and the loading of LSCM, are further optimized. Further characteristic optimization of this NO_2 sensor is under way.

It has been claimed that O_2 as a coexistent gas with NO_2 can intervene sensor response to NO_2 [18,23]. In order to check this point, the influence of different O_2 concentration on the sensor was tested and the results are shown in Fig. 7. In the presence of varying concentration of O_2, a slight increase in current was noted with increasing O_2 concentration. The total increase in current from the change in O_2 between 0% and 10% was only about 1.5%.

In order to further understand the behavior of the sensor with different O_2 concentrations, the impedance spectra were recorded from 1 M to 0.001 Hz with (Fig. 8). The impedance spectra at high frequencies which correspond to the electrolyte behavior, overlapped each other. The result indicates that the impedance values ($|Z|$) of the sensor are hardly affected by gas components, which is consistent with previous studies [10,11]. On the other hand, the impedance value at low frequencies decreased slightly with an increase in the concentration of O_2 in the presence of 300 ppm NO_2. However, the changes of the impedance value in NO_2 concentration from 100 to 300 ppm were by far larger than that in O_2 concentration from 0 to 10% in the presence of 300 ppm NO_2. So, the changes in the low-frequency behavior were much more sensitive to NO_2 than O_2.

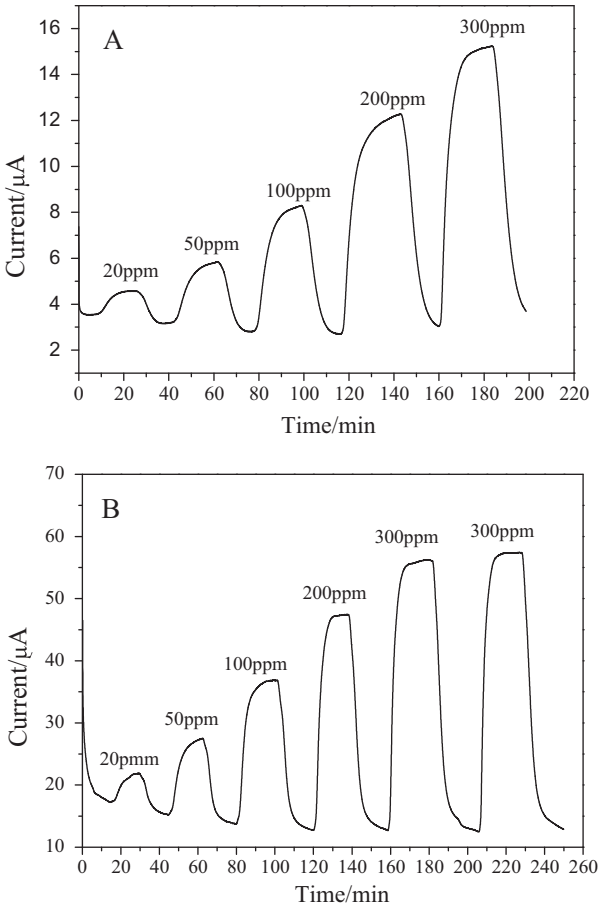

Fig. 5. Amperometric response to 20–300 ppm NO_2 in the presence of 5 vol.% O_2 at 450 °C (A) and 500 °C (B) (applied potential −300 mV, flow rate 100 cm^3/min).

To test the stability of the sensor, the signal of the device was recorded over 3 h upon exposure to 300 ppm NO_2 gas (Fig. 9). It can be found that the current almost kept constant during the test period. When the concentration of NO_2 was switched from 300 to 0 ppm, the sensing current was reversibly returned to the base line which kept stable. The preliminary results reported here imply that the sensor shows good stability. Further research is being carried out for testing the long-term stability and other gas influence.

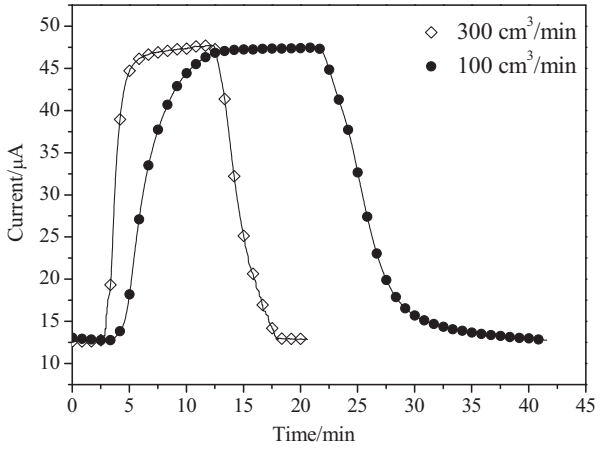

Fig. 6. Amperometric response to 200 ppm NO_2 in the presence of 5 vol.% O_2 at different total flow rates (applied potential −300 mV, 500 °C).

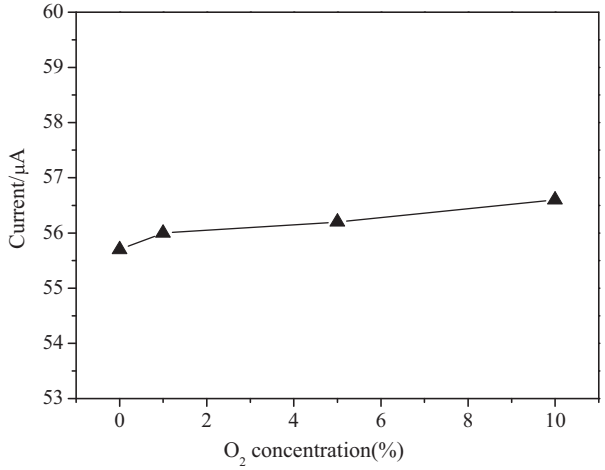

Fig. 7. Dependence of response to 300 ppm NO_2 on concentrations of O_2 (0–10 vol%) for the sensor (applied potential −300 mV, 500 °C).

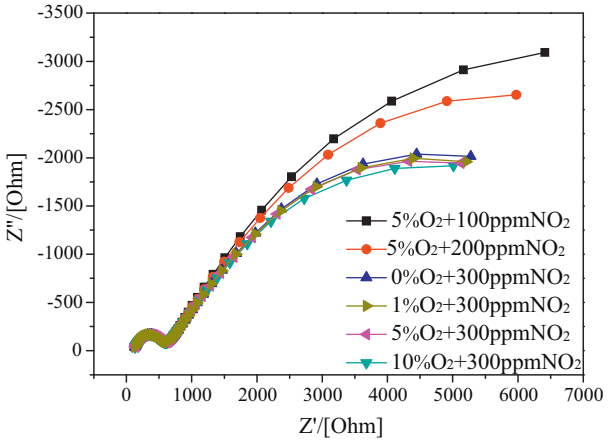

Fig. 8. Nyquist plot of samples with different O_2 concentration in the frequency range of 0.1 Hz to 1 MHz at 500 °C.

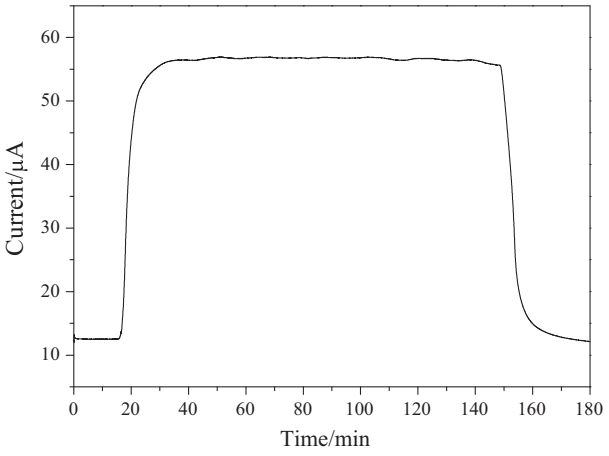

Fig. 9. Stability test for the sensor at 500 °C in the presence of 300 ppm NO_2 (applied potential −300 mV, flow rate 100 cm^3/min).

4. Conclusions

An amperometric NO_2 sensor based on LSCM nano-particles as sensing electrode and CGO as electrolyte was fabricated and tested. The results displayed that the ultrafine LSCM particles were

homogeneously dispersed in the porous CGO layer which greatly increase three phase boundary length (NO_2 gas/LSCM/CGO). The response current was almost linear to NO_2 concentration in the range between 20 and 300 ppm. With the operating temperatures increasing, the sensitivity increases at 400–500 °C. The sensor also shows high reproducibility and good stability. A negligibly increase in response current is noted with increasing O_2 concentration.

Acknowledgements

The authors are grateful to the Natural Science Foundation of China (50972038) and Hebei Provincial Science and Technology Support Program of China (09965119D) support.

References

[1] M. Kampa, E. Castanas, Environ. Pollut. 151 (2008) 362–367.
[2] W. Yang, S.T. Omaye, Mutation Res. 674 (2009) 45–54.
[3] E.D. Bartolomeo, N. Kaabbuathong, A.D. Epifanio, M.L. Grilli, E. Traversa, H. Aono, Y. Sadaoka, J. Eur. Ceram. Soc. 24 (2004) 1187–1190.
[4] P. Elumalai, N. Miura, Solid State Ionics 176 (2005) 2517–2522.
[5] E.R. Macama, B.M. Blackburna, E.D. Wachsmanb, Sens. Actuators B: Chem. 158 (2011) 304–312.
[6] J. Park, B.Y. Yoon, C.O. Park, W.J. Lee, C.B. Lee, Sens. Actuators B: Chem. 135 (2009) 516–523.
[7] N. Miura, J. Wang, M. Nakatou, P. Elumalai, S. Zhuiykov, M. Hasei, Sens. Actuators B: Chem. 114 (2006) 903–909.
[8] E.D. Bartolomeo, M.L. Grilli, J. Eur. Ceram. Soc. 25 (2005) 2959–2964.
[9] M. Stranzenbach, B. Saruhan, Sens. Actuators B: Chem. 137 (2009) 154–163.
[10] L.Y. Woo, L.P. Martin, R.S. Glass, W.S. Wang, S. Jung, R.J. Gorte, E.P. Murray, R.F. Novak, J.H. Visser, J. Electrochem. Soc. 155 (2008) J32–J40.
[11] R. Wama, M. Utiyama, V.V. Plashnitsa, N. Miura, Electrochem. Commun. 9 (2007) 2774–2777.
[12] N. Miura, M. Nakatou, S. Zhuiykov, Sens. Actuators B: Chem. 93 (2003) 221–228.
[13] M. Nakatou, N. Miura, Sens. Actuators B: Chem. 120 (2006) 57–62.
[14] M. Stranzenbach, E. Gramckow, B. Saruhan, Sens. Actuators B: Chem. 127 (2007) 224–230.
[15] T. Ueda, T. Nagano, H. Okawa, S. Takahashi, Electrochem. Commun. 11 (2009) 1654–1656.
[16] A. Dutta, T. Ishihara, Sens. Actuators B: Chem. 108 (2005) 309–313.
[17] P.S. Zhang, W. Zhang, F. Gerlach, K. Ahlborn, U. Guth, Sens. Actuators B: Chem. 108 (2005) 797–802.
[18] J.C. Yang, P.K. Dutta, Sens. Actuators B: Chem. 123 (2007) 929–936.
[19] V. Coillard, L. Juste, C. Lucat, F. Menil, Meas. Sci. Technol. 11 (2000) 212–220.
[20] T. Nakamura, Y. Sakamoto, K. Saji, J. Sakata, Sens. Actuators B: Chem. 93 (2003) 214–220.
[21] V.V. Plashnitsa, P. Elumalai, Y. Fujio, N. Miura, Electrochim. Acta 54 (2009) 6099–6106.
[22] V.V. Plashnitsa, T. Uedab, P. Elumalai, N. Miura, Sens. Actuators B: Chem. 130 (2008) 231–239.
[23] W.Z. Xiong, G.M. Kale, Sens. Actuators B: Chem. 119 (2006) 409–414.
[24] L.P. Martin, L.Y. Woo, R.S. Glass, J. Electrochem. Soc. 154 (2007) J97–J104.
[25] X.S. Liang, S.Q. Yang, J.G. Li, H. Zhang, Q. Diao, W. Zhao, G.Y. Lu, Sens. Actuators B: Chem. 158 (2011) 1–8.
[26] X.B. Zhu, Z. Lü, B. Wei, X.Q. Huang, Y.H. Zhang, W.H. Su, J. Power Sources 196 (2011) 729–733.
[27] S.P. Jiang, Mater. Sci. Eng. A 418 (2006) 199–210.
[28] X.B. Zhu, Z. Lü, B. Wei, K.F. Chen, M.G. Liu, X.Q. Huang, W.H. Su, J. Power Sources 195 (2010) 1793–1798.
[29] C.M. Zhang, Y. Lin, R.R. Zong, P. Shao, Int. J. Hydrogen Energy 35 (2010) 8171–8176.
[30] S. Sridhar, V. Stancovski, U.B. Pal, J. Electrochem. Soc. 144 (1997) 2479–2485.
[31] L. Bay, T. Jacobsen, Solid State Ionics 93 (1997) 201–206.